Observation of moiré superlattices on twisted bilayer graphene by scanning microwave impedance microscopy

Douglas A. A. Ohlberg*[a], Andreij C. Gadelha[b], Diego Tami[c], Eliel G. S. Neto[d], Daniel A. Miranda[b], Jessica S. Lemos[b], Fabiano C. Santana[b], Leonardo C. Campos[b], Jhonattan C. Ramirez[e], Cássio Gonçalves do Rego[e], Ado Jorio[b], Gilberto Medeiros-Ribeiro[f]
[a]Microscopy Center, [b]Physics Department, [c]Electrical Engineering Graduate Program, [e]Department of Electrical Engineering, School of Engineering, [f]Computer Science Department, Universidade Federal de Minas Gerais, Belo Horizonte, MG 31270-901, Brazil.
[d]Instituto de Física, Universidade Federal da Bahia, Campus Universitário de Ondina, Salvador - BA, 40170-115 Brazil.

ABSTRACT

In the emerging field of twistronics, new electronic devices based on bilayer graphene have shown distinct electronic properties that depend on the rotational misalignment of one crystalline layer with respect to another. Given present methods of preparing these bilayers, there is always some uncertainty in the actual versus targeted twist angle of a specific bilayer that can only be resolved by measuring the moiré patterns that are unique to a specific twist angle. Traditional methods enabling such a measurement, Transmission Electron Microscopy and Scanning Tunneling Microscopy, impose serious restrictions on the types of substrates supporting the bilayers, which, in turn, constrains the subsequent fabrication of any devices.

We report here a new, non-destructive method to measure moiré patterns of bilayer graphene deposited on any smooth substrate, using the scanning probe technique known as scanning microwave impedance microscopy (sMIM) which enables the simultaneous generation of localized topography, capacitance and conductance images with nanometer scale resolution[1]. Moiré patterns were observed in samples prepared on various substrates with twist angles ranging from 0.02 to 6.7 degrees, beyond which the moiré patterns are too small to be resolved by the sMIM probes. We present some possible reasons for the various contrast mechanisms. Addressing the problem of variations across a bilayer surface due to localized moiré distortions that result from the tensile and shear forces involved in transferring a twisted bilayer to a substrate, we demonstrate how sMIM can precisely map the twist angle distribution across the film, and enable direct device and circuit routing.

Keywords: Microwave Impedance Microscopy, AFM, bilayer graphene, moiré pattern

1. INTRODUCTION

The discovery of superconducting phases in twisted bilayer graphene (TBG) by the Jarillo-Herrero group in 2018[4] ignited an explosion of interest in 2D Van der Waals material systems that can serve as ideal platforms to study and model correlated systems (Mott insulators, spin liquids, high Tc superconductors, etc.) and topological systems (Quantum Hall effect, topological insulators, etc.). The great appeal of these 2D "twistronic" materials is the relative facility by which they can be constructed layer by layer and electronically tuned by adjustment of the rotational angles between successive layers that are individually perfect, one layer, single-crystals. These systems are presently fabricated using a variety of so-called tear-and-twist techniques in which regions of the relevant material are first ripped loose from a parent mono- or few-layer sheet, rotated and then stacked back on top of the parent layer. The rotational misalignment of the atomic lattice between layers of the resultant structure gives rise to an endless variety of interference patterns, i.e. moiré superlattices whose quasi-periodic structure and electronic properties depend on the lattice parameters of the parent material and angular mismatch between successive layers.

Tear-and-stack methods are at this moment, still far from ideal and can introduce undesirable features such as bubbles, wrinkles, localized variations in the twist angles, and strain into these systems that are detrimental to the yield and

*dohlberg@ufmg.br ; phone (31) 3409-7575; ufmg.br

behavior of devices requiring weeks of fabrication time. There is presently an urgent need for new methods to rapidly and non-invasively screen these structures at the nanometer scale during the various steps of the fabrication process.

Until recently, the only tools capable of characterizing these materials at nanoscales were transmission electron microscopes (TEM) and scanning tunneling microscopes (STM), but these methods are time-consuming and require substrates that are often not compatible with the subsequent fabrication of the multiprobe, gated devices required to probe electronic behavior. Recent developments in Scanning Probe Microscopy (SPM) modalities suggest that more practical means are now available. McGilly et al. have recently demonstrated how piezoforce microscopy (PFM) is able to visualize moiré superlattices with wavelengths less than 5 nm[5]. We report here how another SPM modality, scanning microwave impedance microscopy (sMIM) can quickly image moiré structures of bilayer graphene with periods as small as 2 nm.

2. SCANNING MICROWAVE IMPEDANCE MICROSCOPY

High frequency, near field microscopy has been in constant development ever since the demonstration by Bryant and Gunn in 1965 that microwaves with centimeter scale wavelengths could probe variations in the resistivity of semiconductors with milimeter scale precision[6]. The method has since been incarnated in various scanning probe configurations that have demonstrated nanoscale resolution[7], but until recently, was limited to various laboratories with home-built systems. The development of a batch process for the mass production of specialized, shielded, co-axial AFM probes transformed one embodiment, sMIM, into a modality that today can be implemented in most commercially available AFM systems [1,8].

The sMIM hardware consists of a microwave generator that sends a 3 GHz signal down a two-wire microwave transmission line which terminates in the co-axial AFM tip. As the tip rasters across a surface, collecting data about local topography, localized interactions of the sample with the tip change the amplitude and phase of the reflected signal that travels back up the line to measurement circuitries that measure the amplitudes of the in-phase (real) and out-of-phase (imaginary) components of the reflected signal and route the information to two separate data collection channels. Both of these components are a function of the impedance mismatch between the AFM tip and sample. The real component of the reflected signal is a measurement of the local sample conductivity and the imaginary component, a measurement of the dielectric permittivity of the sample area directly beneath the tip. Although the microwave radiation has a wavelength of around 10 centimeters, the spatial resolution of the technique is limited by the AFM probe size (50 nm radius of curvature), which means that sMIM can be modeled as an evanescent nearfield interaction of tip and substrate.

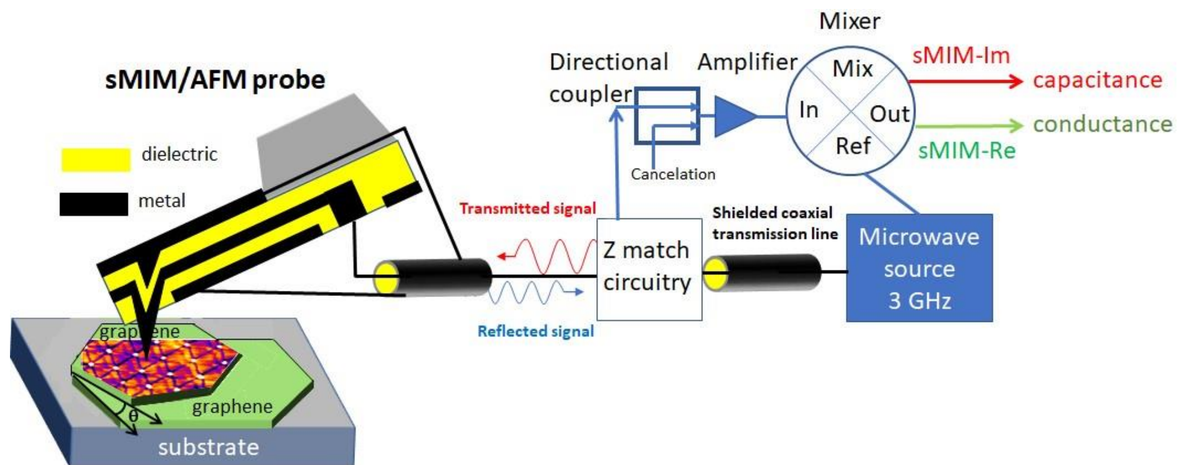

Figure 1. Block diagram of sMIM hardware over twisted bilayer graphene.

3. MOIRÉ SUPERLATTICES IMAGED OVER TWISTED BILAYER GRAPHENE

Samples analyzed by sMIM were prepared using a method recently developed by our group that utilizes a polymer stamp in the form of a truncated pyramid capable of performing tear and stack operations on carbon monolayers without additional adhesive boron nitride thin films or polymers[9]. TBGs were deposited on a variety of substrates that included oxide-coated silicon coupons, glass, glass with boron nitride overlayers, and gold coated mica. Twist angles examined ranged from a few tenths of a degree to 7°. All subsequent sMIM measurements were done under ambient conditions. Previous studies[3] have reported how from 0 degrees up to a critical angle of $\Theta_C \approx 1°$, TBGs undergo atomic reconstruction or relaxation to maximize regions of so-called Bernal AB stacking in which only alternate carbon atoms of the top layer graphene honeycomb sheet are positioned directly over atoms of the underlying bottom sheet. Such a configuration is energetical more favorable than the AA configuration in which every atom of a top hexagon is directly above another atom below. Θ_C is also very close to the magic angle of 1.1° where low temperature correlated insulating and superconducting phases have been observed. For twist angles above Θ_C, atomic reconstruction is energetically too costly, and the bilayers rotate rigidly without relaxation.

In Figure 2, we see the conduction channel images for four TBGs ranging in angles from 0.2° to 6.7°. In Figure 2a patterns consistent with previous reports of TEM images of reconstructed TBGs are observed[2,3]. The triangular regions seen in Figure 2a correspond to the low energy AB/BA regions (nearest neighbor triangles are separated by a mirror plane, and, hence, alternate between AB and mirror symmetric BA stacking). The bright spots at the apices of the triangles correspond to high energy AA stacking sites. The sMIM is also sensitive to the boundaries between AB/BA domains which appear as dark lines in Figure 2a and have been characterized as strain solitons[2] corresponding to localized strain areas in the graphene atomic lattice after reconstruction. In addition to atomic strain, Figure 2a also shows strain in the superlattice structure itself where a distortion or elongation of the reconstruction pattern is observed between the top and bottom halves of the image.

Depending on the quality of the sMIM probe for a specific measurement, we have observed soliton reconstructions at angles as high as 1.5°, shown in Figure 2c, which is higher than any previous reports. In the TBG prepared at the magic angle of 1.1° shown in Figure 2b, although the lattice wavelength of the moiré pattern is easily resolved, it is unclear whether there is any evidence of reconstruction features seen in 2a. This may have to do with the quality of the probe or substrate interactions as the samples in Figures 2b and c were deposited over two different materials. The highest twist angle observed was 6.7°, as shown in Figure 2d, which corresponds to a superlattice period of 2nm. Given the 50 nm radius of tip curvature specified by the probe vendors, the fact that sMIM is able to resolve features twenty-five times smaller is an unexpected surprise requiring further explanation.

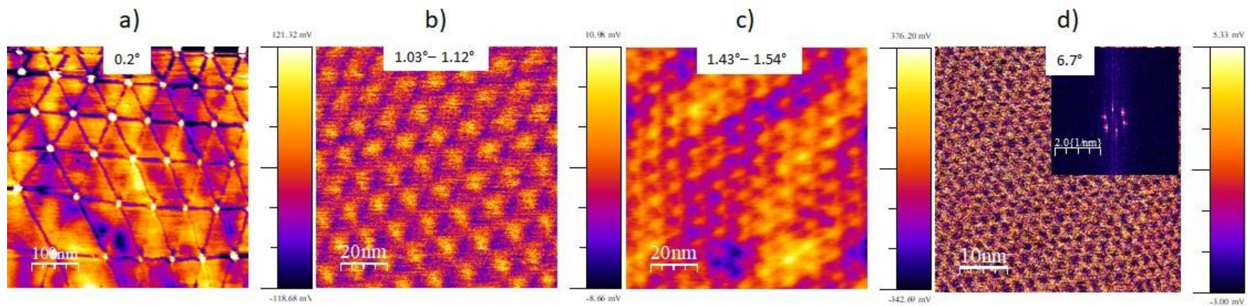

Figure 2. Conductance images of moiré patterns observed over TBG at a) 0.2°, b) near "magic angle" of 1.1°, c) ≈ 1.5°, and d) 6.7°. Inset, Fourier transform of 2d), TBG's in Figures a, b, d were deposited on BN/glass coverslips and c, directly on glass.

4. RESOLUTION AND CONTRAST MECHANISMS

In order to better understand possible mechanisms responsible for the superior spatial resolution of sMIM, COMSOL simulations using multiphysics FEM software were performed to model the electronic displacement field as a function of tip geometry, film thickness and film and substrate permitivities[10].Assuming the simplest model of a tip asperity, the simulations suggest that resolutions on the order of a few nanometers are possible provided the radius of curvature of the

asperity is no more than 5 nm as seen in Figure 3a. The problem of invoking an "asperity" model, however, is that it does not explain why we were able to consistently achieve the same resolutions over the same sample using different tips, each of which would have its own unique nano-scale geometry. This model was also not consistent with the large excursions observed in the capacitance channel traces after the snap-in and snap-off discontinuities of tip-sample approaches that occur when attractive forces cause sudden cantilever deflections towards surfaces during force curve measurements.

One component essential to understanding AFM force curve measurements under ambient conditions is water, which is responsible for the capillary forces that exert such a strong influence on observed cantilever deflection during tip-sample approaches. This has been known for decades and is still a subject of active study measuring and modeling the dynamics of water-meniscus bridge formation between probes and surfaces at nanoscales[11-14]. After inclusion of one nm layer of adventitious water (Figure 3b) and further addition of a proposed meniscus with a radius of curvature of 2 nm[12] in the Comsol simulations (Figures 3c and e), a remarkable concentration of the electric displacement field is observed at air/water boundary of the menisicus, which effectively confines the field to a very small region. In addition to explaining our observed spatial resolution, simulations of the capacitance in which the formation and rupture of a water meniscus bridge were included in the model more closely matched the magnitude of excursions seen in the capacitance signal during force curve measurements[15].

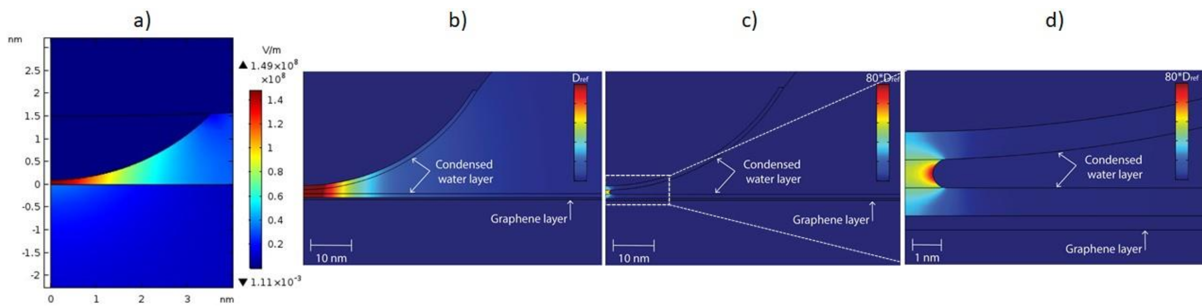

Figure 3. Electric displacement field distribution simulations under various tip/sample regimes. a) 5 nm radius tip asperity without adventitious water. b) 50 nm radius tip with adventitious water. c) Same regime as b after formation of 2nm radius water meniscus. d) Magnification of area around meniscus in c to highlight field concentration.

At present, the underlying physics responsible for contrast mechanisms that make imaging of the moiré patterns possible in the TBG system is still under investigation. Past studies employing scanning tunneling microscopy and scanning tunneling spectroscopy (STS) on a variety of TBGs with various twist angles may suggest a possible explanation[16,17]. In these studies it was found that the tunneling spectra, which are a measurement of the density of states (DOS) show two peaks more or less symmetrical to the Fermi level. These two peaks are Van Hove singularities (VHS) that are a feature of the overlap of the Dirac cones of the top and bottom graphene layers which combine to produce hybridized interlayer bands. The energy spacing between the two VHS corresponds to the energy gap between the saddle points in the valence and conduction band formed by the cone overlap. The energy spacing is linearly proportional to twist angle: At large angles, it increases, and at the magic angle, the spacing essentially collapses with complete overlap of the Dirac cones. It was also shown that the DOS associated with VHS is always higher over AA sites. This has also been demonstrated in localized DOS calculations done by Cao et al. at the magic angle which portray a high concentration of wavefunctions over regions of AA stacking in real space[18]. Local variations in the DOS will cause variation in carrier concentration, and hence conductivity.

The contrast in sMIM may show up in both capacitance and conductance channels, depending on the sample permittivity and conductivity. Samples with higher conductivity exhibit less contrast in both channels, which is intuitively expected as the fields are screened. Calculations that we performed of the real and imaginary components of admittance of our bilayer/meniscus model as a function of sample permittivity and conductivity[15] revealed that for conductivities around 1S/m both channels exhibit maximum contrast, and for low conductance samples, contrast is only observable in the conductance channel.

The capacitance component, however, is comprised of three contributions: a) a geometrical one, which is related to area and radius of curvature of topological features in the sample; b) the sample permittivity, and c) quantum capacitance which is proportional to the DOS. For the TBG cases we can exclude the geometrical contribution as the sample is flat. The conductance is normally associated with the LDOS, which can present contrast if the average conductance is in between 0.1S/m – 10S/m.

Another possible explanation for sMIM imaging comes from a hypothesis proposed by Basov to explain the contrast mechanisms responsible for his piezoforce images[5]. In this explanation, strain gradients centered around AA stacking sites cause out-of-plane distortions in the sp^2 bond orbitals of the graphitic carbon, giving rise to sp^2-sp^3 hybrid orbitals with an out-of-plane polarization similar to that seen in carbon nanotubes that could result in piezoelectric behavior. sMIM should also be sensitive to local polarization changes since the capacitance channel measures local variations in sample permittivity which is a function of polarizability. Interestingly, though, we have observed a number of repeatable cases in which it was only possible to observe contrast in the conductance channel. The opposite case of only observing contrast in the capacitance has not yet been observed to date after surveying dozens of twist angle patterns.

5. SAMPLE SCREENING

Figure 5 illustrates the biggest problem in the present method of TBG preparation through tear-and-stack procedures: inhomogeneity and local variation. Since local variations in strain and twist angle have huge impacts on the band structure of TBG's it is crucial that understanding of electronic behavior observed in area-averaged probes be informed by supplementary measurements with nanoscale probes.

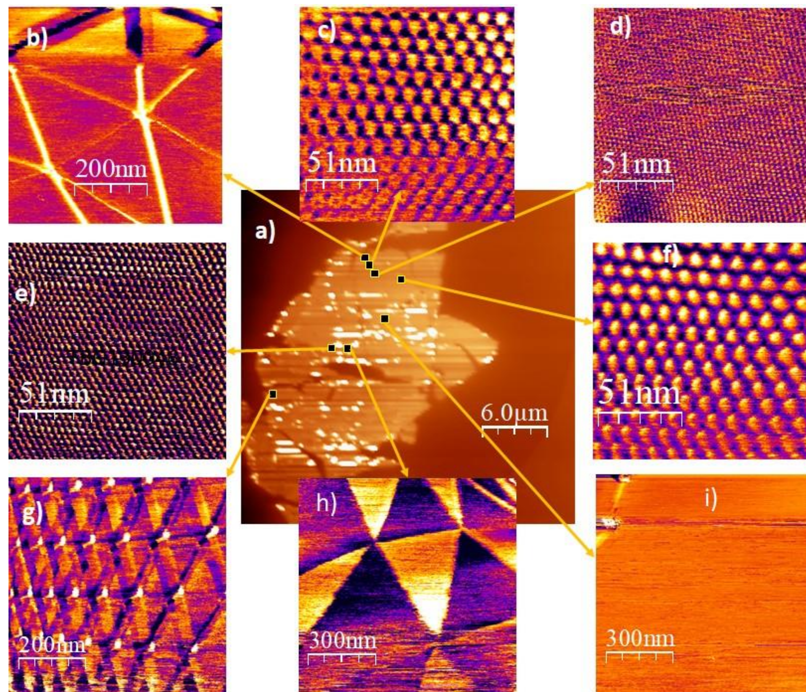

Figure 4. Variations observed in local twist angles of a single TBG deposited on glass with a BN overlayer. a) Capacitance image of complete bilayer. Conductance images of local variations observed in this sample are b) < 0.1°. c) 1.1°. d) 3.4°. e) 2.6°. f) 1.2. g) ≈ 0.2°. h) < 0.1°. i) No pattern except for soliton wall in upper left corner.

Typical examples of area-averaged probes are the four-probe Hall bar devices used by Jarillo-Herrero in his first report of superconductivity[4]. The TBG regions sampled by his devices were several square microns in area and a cursory glance at the TBG in figure 5 shows that devices positioned over any region other than the "magic angle" regions of Figure 4c or 4f would not display correlated behavior. It took years of dogged effort, fabricating countless devices before the Jarillo-Herrero group finally discovered one that demonstrated superconductivity. Today, with the assistance of sMIM as a screening tool, such devices can now be routinely fabricated in less than a week. The data shown in Figure 4 were collected over a few hours under ambient conditions on a bilayer deposited a day earlier over an insulating substrate without any further modification. Although there is considerable variability in the local moiré structure, this feature can now be exploited as a combinatorial platform to systematically explore variation of electronic behavior as a function of well-characterized strain gradients and angular deviations within a single sample.

6. CONCLUSION

We have demonstrated how sMIM can play a major role as a diagnostic tool in the expanding field of twistronics. The list of 2D systems predicted or proven to display emergent, unusual properties is continually growing and includes metals (NbSe2), semi-metals (graphene), semi-conductors (phosphorene, transition metal dichalcogenides, etc.), and insulators (boron nitride). Although the work presented here has exclusively focused on graphene bilayers, there are no obvious reasons why sMIM should not be applicable to these other systems as the technique is fully compatible with conductors, semi-conductors, and insulators. The technique is fast, requires no special conditions for sample preparation, and provides structural characterization with the nano-scale resolution required by the most technologically relevant 2D systems. While the data presented here have mostly been of a qualitative nature, it can also collect quantitative nanoscale information of capacitance and carrier concentration provided the probe is calibrated against suitable reference samples[19,20]. Clearly, the limitations of this technique as a characterization tool in the emerging field of 2D physics are yet to be established.

ACKNOWLEDGEMENTS

The authors acknowledge financial support from CNPq, FINEP, FAPEMIG, INCT Nanomateriais de Carbono, and CAPES.

REFERENCES

[1] Friedman, S.; Amster, O.; Yang, Y.-L.; Recent Advances in Scanning Microwave Impedance Microscopy (sMIM) for Nano-Scale Measurements and Industrial Applications. Proc. of SPIE 9173. 917308-1 (2014).

[2] Alden, J. S., Tsena, A. W., Huanga, P. Y., Hovdena, R., Brown, L., Park, J., Mullera, D. A., and McEuen, P. L., "Strain solitons and topological defects in bilayer graphene", Proc. Natl. Acad. Sci. USA, 110(28), 11256, (2013).

[3] Yoo, H., Engelke, R., Carr, S., Fang, S., Zhang, K., Cazeaux, P., Sung, S. H., Hovden, R., Tsen, A. W.,Taniguchi, T., Watanabe, K., Yi, G.-C., Kim, M., Luskin, M., Tadmor, E. B., Kaxiras, E., Kim, P., "Atomic and electronic reconstruction at the van der Waals interface in twisted bilayer graphene," Nature Materials 18, 448, (2019).

[4] Cao, Y., Fatemi, Valla., Fang, S., Watanabe, K., Taniguchi, T., Kaxiras, E., Jarillo-Herrero, P., "Unconventional superconductivity in magic-angle graphene superlattices," Nature, 556, 43, (2018).

[5] Mcgilly, L. J., Kerelsky, A., Finney, N. R., Shapovalov, K., Shih, E-M., Ghiotto, A., Zeng, y., Moore, S. L., Wu, W., Bai, Y., Watanabe, K., Taniguchi, T., Stengel, M., Zhou, L., Hone, J., Zhu, X., Basov, D. N., Dean, C., Dreyer, C. E., Pasupathy, A. N.,"Visualization of moiré superlattices," Nature Nanotechnology, June (2020).

[6] Rosner, B. T., van der Weide, D. W., "High-frequency near-field microscopy", Rev. Sci. Instrum. 73(7), 2505, AIP (2002).

[7] Lai, K., Kundhikanjana, W., Kelly, M., Shen, Z. X., “Modeling and characterization of a cantilever-based near-field scanning microwave impedance microscope,” Rev. Sci. Instrum. 79, 063703, AIP (2008).
[8] Yang, Y., Lai, K., Tang, Q., Kundhikanjana, W., Kelly, M. A., Zhang, K., Shen, Z.., Li, X., “Batch-fabricated cantilever probes with electrical shielding for nanoscale dielectric and conductivity imaging,” J. Micromechanics Microengineering 22(11), 115040 (2012).
[9] Gadelha, A. C., Ohlberg, D. A. A., Rabelo, C., Neto, E. G. S., Vasconcelos, T. L., Campos, J. L., Lemos, J. S., Ornelas, V., Miranda, D., Nadas, R., Santana, F. C., Watanabe, K., Taniguchi, T., van Troeye, B., Lamparski, M., Meunier, V., Nguyen, V.-H., Paszko, D., Charlier, J.-C., Campos, L. C., Cançado, L. G. Medeiros-Ribeiro, G., Jorio, A., “Lattice dynamics localization in low-angle twisted bilayer graphene.” arXiv:2006.09482 (2020).
[10] Volakis, J. L., Chatterjee, A.,Kempel, L. C. Finite Element Method Electromagnetics: Antennas, Microwave Circuits, and Scattering Applications. Wiley Interscience (1998).
[11] Kwon, S., Kim, B., An, S., Lee, W., Kwak, H.-Y., Jhe, W.,” Adhesive force measurement of steady-state water nano-meniscus: Efective surface tension at nanoscale,” Sci. R., 8:8462 (2018).
[12] Szoszkiewicz, R., Riedo, E., “Nucleation time of nanoscale water bridges,” Phys. Rev. Let., 95(13) (2005).
[13] Carpentier, S., Rodrigues, M. S., Vitorino, M. V., Luca Costa, Charlaix, E., Chevrier, J., “Out of equilibrium anomalous elastic response of a water nano-meniscus,” Ap. Phys. Let., 107(20):204101 (2015).
[14] Jang, J., Schatz, G. C., Ratner, M. A., “How Narrow Can a Meniscus Be?” Phys. Rev. Let., 92(8), 085504-1, (2004).
[15] Ohlberg, D. A. A., Tami, D., Gadelha, A. C., Neto, E. G. S., Santana, F. C., Miranda, D., Avelino, W., Watanabe, K.,Taniguchi, T., Campos, L. C., Ramirez, J. C., Gonçalves do Rego, C., Jorio, A., Medeiros-Ribeiro, G.,” The limits of Near Field Immersion Microwave Microscopy evaluated by imaging bilayer graphene Moiré patterns,” arXiv:2007.03823 (2020).
[16] Li, G., Luican, A. J., Lopes dos Santos, M. B., Castro Neto, A. H., Reina, A., Kong, J., Andrei, E. Y., “Observation of Van Hove singularities in twisted graphene layers,” Nature Phys., 6, 109 (2009).
[17] Yan, W., Meng, L., Liu, M., Qiao, J.-B., Chu, Z.-D., Dou, R.-F., Liu, Z., Nie, J.-C., Naugle, D, G., He, L., “Angle-dependent van Hove singularities and their breakdown in twisted graphene bilayers” Phys. Rev. B. 90, 115402 (2014).
[18] Cao, Y., Fatem, V., Demir, A., Fang, S., Tomarken, S. L., Luo, J. Y., Sanchez-Yamagishi, J. D., Watanabe, K., Taniguchi, T., Kaxiras, E., Ashoori, R. C., Jarillo-Herrero, P.,” Correlated insulator behaviour at half-filling in magic-angle graphene superlattices,” Nature, 556, 80 (2018).
[19] Huber, H. P., Moertelmaier, M. , Wallis, T. M., Chiang, C. J., Hochleitner, M., Imtiaz, A., Oh, Y. J., Schilcher, K., Dieudonne, M., Smoliner, J., Hinterdorfer, P., Rosner, S. J., Tanbakuchi, H., Kabos, P., Kienberger, F., “Calibrated nanoscale capacitance measurements using a scanning microwave microscope”, Rev. Sci. Instrum. 81, 113701, AIP (2010).
[20] Huber, H. P., Humer, I., Hochleitner, M., Fenner, M., Moertelmaier, M., Rankl, C., Imtiaz, A., Wallis, T. M., Tanbakuchi, H., Hinterdorfer, P., Kabos, P., Smoliner, J., Kopanski, J. J., Kienberger, F., “Calibrated nanoscale dopant profiling using a scanning microwave microscope,” J. Appl. Phys. 111, 014301 (2012).